ChemComm

Accepted Manuscript

This article can be cited before page numbers have been issued, to do this please use: N. Kurra, C. Xia, M. N. Hedhili and H. N. Alshareef, *Chem. Commun.*, 2015, DOI: 10.1039/C5CC03220B.

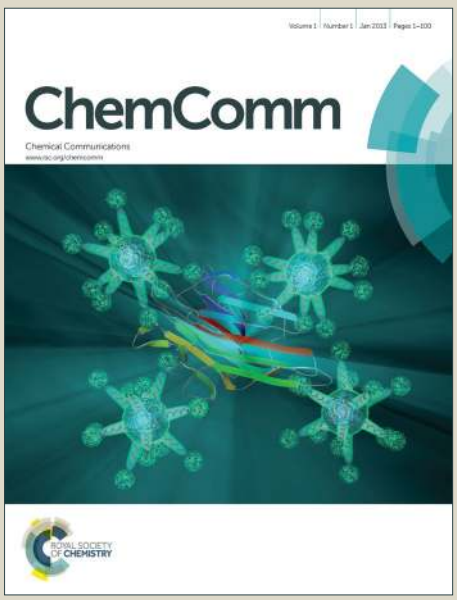

This is an *Accepted Manuscript*, which has been through the Royal Society of Chemistry peer review process and has been accepted for publication.

Accepted Manuscripts are published online shortly after acceptance, before technical editing, formatting and proof reading. Using this free service, authors can make their results available to the community, in citable form, before we publish the edited article. We will replace this *Accepted Manuscript* with the edited and formatted *Advance Article* as soon as it is available.

You can find more information about *Accepted Manuscripts* in the Information for Authors.

Please note that technical editing may introduce minor changes to the text and/or graphics, which may alter content. The journal's standard Terms & Conditions and the Ethical guidelines still apply. In no event shall the Royal Society of Chemistry be held responsible for any errors or omissions in this *Accepted Manuscript* or any consequences arising from the use of any information it contains.

ROYAL SOCIETY OF CHEMISTRY

www.rsc.org/chemcomm

View Article Online
DOI: 10.1039/C5CC03220B

Journal Name

COMMUNICATION

High Performance Ternary Nickel Cobalt Sulfide Micro-pseudocapacitor

*Narendra Kurra[+], Chuan Xia[+], M. N. Hedhili and H. N. Alshareef**

Received 00th January 20xx,
Accepted 00th January 20xx

DOI: 10.1039/x0xx00000x

www.rsc.org/

We report the successful fabrication of a micro-pseudocapacitor based on ternary nickel cobalt sulfide for the first time, with performance substantially exceeding that of previously reported micro-pseudocapacitors based on binary sulfides. $CoNi_2S_4$ micro-pseudocapacitor exhibits a maximum energy density of 18.7 mWh/cm^3 at a power density of 1163 mW/cm^3, opens up an avenue for exploring new family of ternary oxides/sulfides based micro-pseudocapacitors.

Microsupercapacitors (MSCs) are promising devices for next generation on-chip energy storage due to their high power density, which can complement high energy density batteries.[1-3] Additional attributes of MSCs include excellent rate capability, long cycling lifetime, and superior volumetric capacity to their conventional sandwich counter-parts.[3,4] The planar configuration of MSCs can allow robust integration with functional electronic devices such as microsensors and biomedical implants as micro-power units.[5-7] Hence, a great deal of research has been focused on a variety of nanostructured electroactive materials that are amenable to fabricate in-plane MSCs.[3,4]

Various MSCs based on conducting porous carbon were fabricated employing conventional photolithography and deposition or etching schemes. For example, high surface area carbon forms such as activated,[8] carbide derived,[2] onion like[9] and carbon nanotubes[10] have been patterned employing photolithography followed by deposition methods such as ink-jet printing, electrophoretic and spray deposition. Further, high temperature chemical vapor deposition (CVD) was also employed in growing carbon nanotubes (CNTs) and graphene or both selectively over the patterned current collectors.[11,12] Of late, due to compatible solution processability, graphene oxide (GO) has become attractive candidate material for making MSCs employing etching scheme in a photolithography technique[13] or innovative direct laser scribing methods.[14,15] Further, in order to improve the limited capacitance of carbon based MSCs, several pseudocapacitive materials including metal oxides/hydroxides (RuO_2, MnO_2 and $Ni(OH)_2$),[16-18] and even conducting polymers (PPY, PANI, PEDOT)[19-22] were employed to fabricate high capacity micro-pseudocapacitors. These pseudocapacitive materials can undergo fast redox reactions at their nanostructured surfaces, contributing to the higher values of capacity and hence energy density.[16-22]

Recently, new electrode materials in the form of binary and ternary sulfides have been explored as potential candidates for pseudocapacitors.[23-25] However, most of the studies have been focused on synthesis and investigating their electrochemical performance in 3-electrode configuration. To exploit the practical usage of these new materials, it is highly desirable to build energy storage devices in a 2-electrode configuration.[25,26] In-plane MSCs based on binary metal sulfides such as MoS_2 and VS_2 have been fabricated which showed an areal cell capacitance of 5-8 mF/cm^2.[27,28] Moreover, nanostructured sulfides, in particular, ternary nickel cobalt sulfides have become outstanding electrode materials due to their higher conductivity richer redox reactions than the single component sulfides due to contributions from nickel and cobalt ions.[23-25] In addition, it was demonstrated that these ternary cobalt nickel sulfides exhibit higher electronic conductivity and richer redox reactions than their ternary oxide counter-parts, resulting in higher capacity values.[29] Here, we demonstrate the fabrication of ternary sulfide micro-pseudocapacitors with excellent volumetric capacitance and energy density.

We report the fabrication of nanostructured ternary cobalt nickel sulfide micro-pseudocapacitor employing electrochemical co-deposition over the rGO/Au/patterned photoresist. The rGO free-standing films are prepared through vacuum filtration from its dispersion. Before doing lift-off, ternary cobalt nickel sulfide was electrodeposited to ensure uniform deposition over the entire area. The resulting $CoNi_2S_4$ MSC exhibits a volumetric capacitance of 211 F/cm^3 (areal capacitance of 11.6 mF/cm^2), corresponding to an energy density of 18.7 mWh/cm^3 at a power density of 1163 mW/cm^3. This is the best reported performance of any sulfide based micro-pseudocapacitor.

Glass substrates (Fischer) were cut into 1x1'' size, cleaned with a soap solution to remove the dirt or grease followed by sonicating in acetone, isopropanol and deionized water sequentially for 5 minutes each and then dried by blowing nitrogen. Positive photoresist AZ9260 was spun coated at 3000 rpm for 60 seconds over the glass substrates to get 10 µm thick photoresist layer. Photoresist coated substrates were soft baked at 110 ºC for 3 minutes. Ultra-Violet (UV) exposure was done using EVG contact aligner at a constant dose of 1800 mJ/cm^2 through the Cr/Glass mask having the interdigitated patterns. After the exposure, samples were developed in AZ726 developer solution for 6 minutes, which resulted in the formation of patterns in the photoresist layer. Metal layers of 200 nm Au/20 nm Ti were deposited by sputtering (Equipment Support Co., Cambridge, England) technique over the patterned photoresist layer. Before the lift-off process, free-standing rGO film obtained through vacuum filtration was transferred onto metal-coated patterned photoresist followed by electrochemical co-deposition of nickel cobalt sulfide.[25]

[a] *Address here.*
[b] *Address here.*
[c] *Address here.*
† Footnotes relating to the title and/or authors should appear here.
Electronic Supplementary Information (ESI) available: [details of any supplementary information available should be included here]. See DOI: 10.1039/x0xx00000x

View Article Online
DOI: 10.1039/C5CC03220B

Graphite oxide was prepared from natural graphite source using a modified Hummers method.[30] Thus obtained graphite oxide was exfoliated in de-ionized (DI) water by sonicating using a bath sonicator (UP400S, Ultrasonic processor; Hielscher ultrasound Technology) for 1hr. The resulting graphene oxide was then reduced to graphene by following a method reported by Li et al.[31] The supernatant solution containing thin layers of graphene was used for obtaining free-standing rGO films. The rGO dispersion was filtered using vacuum filtration (VF) method on a porous alumina membrane filter (0.2 µm pore size and 25 mm diameter; Whatman).[32] The alumina membrane was removed by dissolving it into a bath of 3M NaOH solution in order to obtain free-standing rGO film. This film was then transferred to a water bath to remove the traces of adsorbed NaOH over the rGO surface and this step was repeated for several times. Finally, rGO film was transferred onto the Au-coated patterned photoresist chip followed by drying off in a heating oven at 60 ºC for 3 minutes.

An optimized recipe reported in the reference 25 was employed for electrochemical co-deposition, consists of 5 mM $CoCl_2.6H_2O$ with 7.5 mM $NiCl_2.6H_2O$ and 0.75 M thiourea ($CS(NH_2)_2$), resulting in the $CoNi_2S_4$. The pH value of the solution was adjusted with diluted $NH_3{\cdot}H_2O$ to ~6. The potentiodynamic deposition was carried out in a three-electrode cell using rGO/Au coated patterned photoresist, Pt as counter, and Ag/AgCl as reference electrodes by cyclic voltammetry at a scan rate of 5 mV/s for 1-6 cycles within a potential range of -1.2 to 0.2 V vs. Ag/AgCl.[25] After the electrodeposition, substrates were cleaned by rinsing with water to remove unreacted initial precursor solution, followed by drying in air and drying at 60 ºC for 3 min.

Surface morphology and microstructure were imaged by scanning electron microscope (SEM) (Nova Nano 630 instrument, FEI Co., The Netherlands). The film thicknesses were measured using a Veeco Dektak 150 surface profilometer. X-ray photoelectron spectroscopy (XPS) analysis was carried out in a Kratos Axis Ultra DLD spectrometer equipped with a monochromatic Al K_α X–ray source (hv = 1486.6 eV) operating at 150 W, a multi-channel plate and delay line detector under a vacuum of ~10^{-9} mbar. The high-resolution spectra were collected at fixed analyzer pass energy of 20 eV.

The electrochemical performance of $CoNi_2S_4$/rGO MSCs was investigated in a 2-electrode configuration using an electrochemical workstation (CHI 660D, CH Instruments Incorporation). Cyclic voltammetry (CV), galvanostatic charge-discharge (CD), and electrochemical impedance spectroscopy (EIS) measurements were carried out in 1M KOH electrolyte. CV experiments were carried out at different scan rates selected from 0.01 to 50 V/s. CD experiments were performed using current densities selected from 60 to 320 µA/cm^2. The electrochemical impedance spectroscopy (EIS) was measured using a Modulab (Solartron Analytical) electrochemical workstation in the frequency range from 100 kHz to 0.1 Hz at open circuit potential by applying a small sinusoidal potential of 10 mV signal. Electrochemical cycling stability was measured using VMP3 multichannel electrochemical workstation (Bio-Logic). All measurements were done at room temperature.

Figure 1a shows the rGO dispersion (described in the experimental section) that was used to obtain rGO thin films by vacuum filtration over anodic alumina membrane. The alumina membrane was subsequently dissolved away in 3M NaOH to result in the freely floating film of rGO over the water bath as shown in Fig. 1b. This rGO film is comprised of tightly packed small flakes (lateral dimensions, 200 nm) giving rise to innumerable edges, domain boundaries, and interfaces. Raman spectrum of rGO film shows broad D and G bands centered at 1367 (FWHM, 206 cm^{-1}) and 1598cm^{-1} (FWHM, 91 cm^{-1}), respectively. The D band originates form the presence of defects and functional groups while the G band corresponds to symmetric stretching of sp^2 carbon lattice with E_{2g} symmetry.[33] The I_D/I_G ratio of rGO films was found to be in the range of 0.8-0.9 and the sp^2 crystallite size was estimated using below the formula,[34] found to be 10-15 nm. E_{laser} is the laser excitation energy (eV) in the following equation.

$$L_a(nm) = 560/E^4_{laser}(I_D/I_G)^{-1} \quad \text{.....(I)}$$

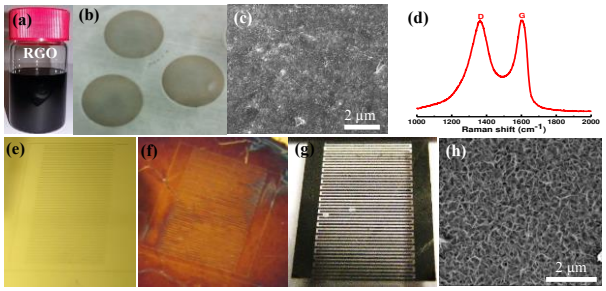

Fig. 1 Digital photographs showing (a) rGO dispersion, (b) freely floating rG thin film obtained through vacuum filtration. (c) SEM micrograph showing the morphology of rGO film. (d) Raman spectrum of rGO. Photograp s showing (e) Au coated patterned photoresist, (f) transferring of rGO onto Au/patterned photoresist, (g) electrochemical co-deposition of Co followed by lift-off in resulting $CoNi_2S_4$ interdigitated electrodes. (h) nanostructured morphology of $CoNi_2S_4$.

We have followed conventional photolithgoraphy lift-off protoco fabricate ternary nickel cobalt sulfide micro-pseudocapacitors (Detail fabrication process is illustrasted in the electronic supplementary information, Fig. S1). Initially, metal coated patterned photoresist chip w employed as a platform to transfer free-standing rGO film as shown in Fig 1e and 1f. Reduced graphene oxide (rGO) provides a functional conducti graphitic platform which, when used as current collector, improves the nucleation and growth of pseudocapacitive materials compared to met current collectors.[35] Recently, Du et al. have demonstrated a physic approach in synthesizing nanocomposite of $CoNi_2S_4$/graphene with excellent electrochemical performance.[36] We have found that compared to the met surfaces such as Au or Ni, functional rGO surface helps in the uniform growth of ternary sulfides (Fig. S2, ESI). It was observed that the growth $CoNi_2S_4$ was non-uniform over the Au current collectors as evident from th SEM micrographs shown in Fig. S2. However, Au acts as a conductiv support/current collector while rGO layer helps in the homogenous a uniform nucleation and growth of $CoNi_2S_4$ during electrochemical co-deposition process. Electrochemical co-deposition was carried out before doing the photoresist lift-off to ensure uniform electric field and uni growth of $CoNi_2S_4$ over the entire chip. Doing the resist lift-off before electrodeposition would have created irregular electric fields and non-uniform growth of the $CoNi_2S_4$. The strong adherence of nickel cobalt sulfide onto the rGO film is evident since the final step of lift-off involved rigoro ultrasonication to make the $CoNi_2S_4$/rGO finger electrodes. It is obvious fro the SEM micrograph shown in the Fig. 1h the electrodeposited $CoNi_2S_4$ lay has a uniform monolithic morphology. We have considered rGO thin film as a platform for growing $CoNi_2S_4$ heterostructures with interdigitat electrode patterns in evaluating its electrochemical performance in a electrode configuration.

XPS analysis was carried out in order to determine the chemical composition of the sample and the oxidation state of detected elements. High resolution XPS spectra of Co 2p, Ni 2p, and S 2p core levels have been recorded an are shown in Fig. 2. The high resolution XPS spectra match well with th obtained for ternary nickel cobalt sulfides $CoNi_2S_4$[37] and $NiCo_2S_4$.[38,39] Precise distinction between the two sulfides is difficult due to the similarities of th shape and binding energies of the Co 2p, Ni 2p and S 2p core levels. Th elemental composition was obtained using XPS by applying the appropriat relative sensitivity factors (RSFs) to the integrated peak areas of specific core levels for the different elements. The atomic ratio S/Ni/Co was estimated to be 4:2:1, which can be assigned to $CoNi_2S_4$. The Ni $2p_{3/2}$ portion of the Ni 2p spectrum was fitted using three components.

The Ni $2p_{3/2}$ components observed at 852.9 and 855.7 eV correspond to Ni^{2+} and Ni^{3+} species, respectively.[37,40] The third Ni $2p_{3/2}$ component located at 861.3 eV is related to a shake-up satellite of Ni^{3+} species.[37,40] The Co $2p_{3/2}$ part of the Co 2p spectrum was fitted using three components as well. The Co $2p_{3/2}$ component observed at 778.2 is attributed to Co^{3+} species, while the components located at 781.0, and 786. 3 eV correspond to Co^{2+} main peak accompanied with its shake-up satellite, respectively.[37,40] For the S 2p high resolution XPS spectrum, the peak observed at 161.3 eV corresponding to S $2p_{3/2}$ core level wich is typical of metal sulfur bounds in the ternary metal sulfides[41] and consistent with nickel and cobalt sulfides.[41] The S 2p peak observed at 168.0 eV is attributed to surface sulfur with high oxide state, such as sulfates.

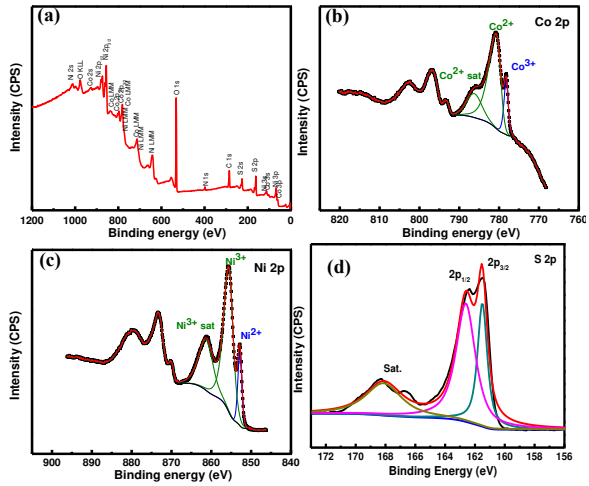

Fig. 2. X-ray photoelectron spectroscopy (XPS) of $CoNi_2S_4$ (a) survey scan and core-level spectra of (b) Co 2p, (c) Ni 2p and (d) S 2p.

The electrochemical performance of $CoNi_2S_4$ micro-pseudocapacitor was tested in 2-electrode configuration in 1M KOH electrolyte. Unlike the EDLC behavior of rGO MSC where the charge is stored through the electrostatic accumulation of electrolytic ions, redox behavior from the $CoNi_2S_4$ MSC is observed (see Fig. S3, ESI). As shown in Fig. 3a, the redox peaks appear at different scan rates, due to redox behavior of $Co^{+4}/Co^{+3}/Co^{+2}$ and Ni^{+3}/Ni^{+2} couples, mediated by the hydroxyl ions (OH^-) in the electrolyte. Since sulfur belongs to same group of oxygen, OH^- ions can induce electrochemical oxidation and reduction of $CoNi_2S_4$ in alkaline medium similar to that of metal oxides/hydroxides. However, it is difficult to deconvlute the contributions of Ni and Co due to broad nature of redox peaks, most probably due to reversible formation of redox couples such as NiS/NiS(OH) and CoS/CoS(OH)/CoSO. At a scan rate of 10 mV/s, $CoNi_2S_4$ shows an areal cell capacitance of 11.6 mF/cm^2, which is superior to binary metal oxide (areal cell capacitance of 1-5 mF/cm^2) and sulfide (VS_2, MoS_2; C_A = 4-8 mF/cm^2) based micro-pseudocapacitors. It was found that the areal capacitance was gradually increasing from 1.7 to 11.6 mF/cm^2 (at a current density of 160 μA/cm^2) due to more loading of $CoNi_2S_4$ when the deposition cycles were increased from 1 to 6 (see Fig. S4, ESI). Due to the planar configuration of the $CoNi_2S_4$ interdigitated electrodes, CVs were recorded even at higher scan rates of 1-50 V/s as shown in Fig. 3c. Similarly, charge-discharge curves of $CoNi_2S_4$ MSC at different current densities were recoded as shown in Fig. 3d. CD profiles are highly non-linear, clearly demonstrating the pseudocapacitive behavior the $CoNi_2S_4$ electrodes. We have found that this micro-pseudocapacitor exhibits an areal cell capacitance of 11.6 mF/cm^2 (thickness of $CoNi_2S_4$/rGO is about 0.55 μm) which corresponds to a volumetric capacitance of 211 F/cm^3. While pristine rGO based MSC shows a much lower areal capacitance of 0.3 mF/cm^2 with a volumetric capacitance of 40 F/cm^3. Cycling stability of $CoNi_2S_4$ MSC was tested by continuous charging/discharging at a current density of 320 μA/cm^2 which showed a capacitance retention of 80% after 5000 cycles with a Coulombic efficiency above 95% (see Fig. S5, ESI). Further, solid state $CoNi_2S_4$ MSC was fabrica... by employing PVA/KOH gel electrolyte which exhibits an areal capacitance of 2.8 mF/cm^2 (see Fig. S6, ESI). Thus, enhanced values of areal a... volumetric capacitance of $CoNi_2S_4$ MSC is due to pseudocapacitive natur... unlike the EDLC behavior of carbon based MSCs. This volumetric capacit... is still higher than MoS_2 MSC (178 F/cm^3). Thus, these ternary $CoNi_2S_4$ wi... impressive redox contributions from the Ni and Co metals as well as facile ionic diffusion through the nanostructured electrodes give rise to high... volumetric capacitance. Impedance spectrum for $CoNi_2S_4$ micro... pseudocapacitor is shown in Fig. 3e. The presence of semi-circle in the high frequency region is due to charge-transfer resistance across the electrode/electrolyte interface with an equivalent series resistance (ESR) o... 5 Ω (see inset of Fig. 3e). An optimized $CoNi_2S_4$ micro-pseudocapacit... exhibits a maximum energy density of 18.7 mWh/cm^3 at a power density of 1163 mW/cm^3. The energy density values are at least twice that of carbon,[15] and metal oxide based MSCs[16,17] (E = 1-10 mWh/cm^3) fabricated in th... literature. As shown in the Ragone plot in Fig. 3f, $CoNi_2S_4$ MSC exhibi... superior energy density over the binary sulfide based MSCs such as MoS_2 (E = 6 mWh/cm^3)[27] and VS_2 (E = 15 mWh/cm^3) (see Table S1, ESI).[28] The ... $CoNi_2S_4$ MSCs exhibit a maximum power density of 2327 mW/cm^3 even at an... energy density of 14.2 mWh/cm^3. This study opens up possibilit... employing ternary sulfides as potential candidate electrode materials for on-... chip energy storage with superior volumetric capacitance and en... density.

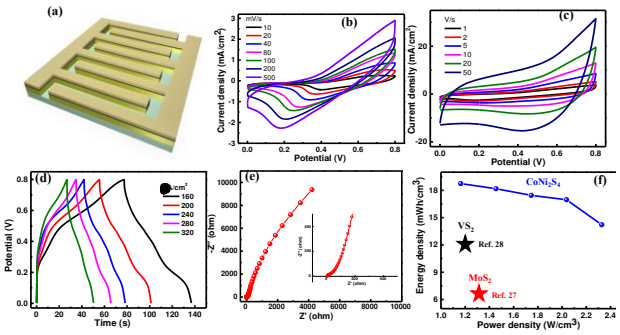

Fig. 3 (a) Schematic showing the interdigitated electrodes of $CoNi_2S_4$. (b) an... (c) CVs of $CoNi_2S_4$ MSC in 1M KOH in 2-electrode configuration. (d) Charge-discharge curves at different current densities. (e) Impedance spectra of ... device, inset shows high frequency region of the spectrum. (f) Ragone pl... comparing the energy and power densities of $CoNi_2S_4$ micro-pseudocapacitor with respect to MoS_2 and VS_2 micro-pseudocapacitors reported in the literature.

In summary, we have demonstrated the successful fabrication of micro-pseudocapacitors based on ternary nickel cobalt sulfides. This was achieve... by employing single-step electrochemical co-deposition of nickel coba... sulfide over transferred reduced graphene oxide (rGO) thin films followed b... photo resist lift-off. The fabricated $CoNi_2S_4$ micro-pseudocapacitors exhibit a maximum areal cell capacitance of 11.6 mF/cm^2 with a volumetr... capacitance of 211 F/cm^3. The maximum energy density of 18.7 mWh/cm^3 ... a power density of 1163 mW/cm^3 was achieved, which is superior to the binary sulfide micro-supercapacitors reported in the literature. This s...dy may open up an opportunity to fabricate various kinds of ter...ary oxides/sulfides based micro-pseudocapacitors.

Research reported in this publication was supported by King Abdulla... University of Science and Technology (KAUST). Authors thank the Advanced Nanofabrication, Imaging and Characterization Laboratory at KAUST for the... excellent support.

Notes and references

Material Science and Engineering, King Abdullah University of Science and Technology (KAUST), Thuwal 23955-6900, Saudi Arabia
E-mail: husam.alshareef@kaust.edu.sa
+contributed equally to the work

† Electronic Supplementary Information (ESI) available. See DOI: 10.1039/c000000x/

1 P. Simon and Y. Gogotsi, *Nat. Mater.*, 2008, 7, 845.
2 J. Chmiola, C. Largeot, P. L. Taberna, P. Simon and Y.Gogotsi, *Science*, 2010, **328**, 480.
3 M. Beidaghi and Y. Gogotsi, *Energy Environ. Sci.,* 2014, **7**, 867.
4 G. Xiong, C. Meng, R. G. Reifenberger, P. P. Irazoqui and T. S. Fisher, *Electroanalysis,* 2014, **26**, 30.
5 F. Simjee, P. H. Chou, In *Everlast: Long-life, Supercapacitor-operated Wireless Sensor Node*, Low Power Electronics and Design, 2006. ISLPED'06. Proceedings of the 2006 International Symposium on, 4-6 Oct. 2006; 2006; pp 197-202.
6. Z. L. Wang, Adv. Mater., 2012, 24, 280–285.
7. Z. L. Wang and W. Wu, Angew. Chem., Int. Ed., 2012, 51, 11700–11721.
8. D. Pech, M. Brunet, P. L. Taberna, P. Simon, N. Fabre, F. Mesnilgrente, V. Con´ed´era and H. Durou, *J. Power Sources,* 2010, **195**, 1266.
9. D. Pech, M. Brunet, H. Durou, P. Huang, V. Mochalin, Y. Gogotsi, P.-L. Taberna and P.Simon, *Nat. Nanotechnol.,* 2010, **5**, 651.
10. M. Beidaghi and C. L. Wang, *Adv. Funct. Mater.,* 2012, **22**, 4501.
11. J. Lin, C. Zhang, Z. Yan, Y. Zhu, Z. Peng, R. H. Hauge, D. Natelson and J. M. Tour, *Nano Lett.,* 2012, **13**, 72.
12. G. Xiong, C. Meng, R. G. Reifenberger, P. P. Irazoqui and T. S. Fisher, *Energy Technology* 2014, **2**, 897.
13 Z. S. Wu, K. Parvez, X. Feng and K. Müllen, *Nat. Commun.,* 2013, **4***,* 2487.
14 W. Gao, N. Singh, L. Song, Z. Liu, A. L. M. Reddy, L. Ci, R. Vajtai, Q. Zhang, B. Wei and P. M. Ajayan, *Nat. Nanotechnol.,* 2011, **6**, 6.
15 M. F. El-Kady and R. B. Kaner, *Nat. Commun.,* 2013, **4**, 1475.
16 T. M. Dinh, K. Armstrong, D. Guay and D. Pech, *J. Mater. Chem. A,* 2014, **2**, 7170.
17 W. Si, C. Yan, Y. Chen, S. Oswald, L. Han and O. G. Schmidt, *Energy Environ. Sci.,* 2013, **6**, 3218.
18 N. Kurra, N. A. Alhebshi and H. N. Alshareef, *Adv. Energy Mater.,* 2014, **4**, 1401303.
19 M. Beidaghi and C. L. Wang, *Electrochim. Acta,* 2011, **56**, 9508.
20 K. Wang, W. Zou, B. Quan, A. Yu, H. Wu, P. Jiang and Z. Wei, *Adv. Energy. Mater.*, 2011, **1**, 1068.
21 C. Meng, J. Maeng, S. W. M. John and P. P. Irazoqui, *Adv. Energy. Mater.,* 2014, **4**, 1301269.
22 N. Kurra, M. K. Hota and H. N. Alshareef, *Nano Energy*, 2015, **13**, 500.
23 H. Wan, J. Jiang, J. Yu, K. Xu, L. Miao, L. Zhang, H. Chen and Y. Ruan, CrystEngComm, 2013, 15, 7649.
24 S. Peng, L. Li, C. Li, H. Tan, R. Cai, H. Yu, S. Mhaisalkar, M. Srinivasan, S. Ramakrishna and Q. Yan, Chem. Commun., 2013, 49, 10178.
25 W. Chen, C. Xia, and H. N. Alshareef, *ACS Nano*, 2014, **8**, 9531.
26 M. D. Stoller, R. S. Ruoff, *Energy Environ. Sci.* 2010, 3, 1294.
27 L. Cao, S. Yang, W. Gao, Z. Liu, Y. Gong, L. Ma, G. Shi, S. Lei, Y. Zhang, S. Zhang, R. Vajtai and P. M. Ajayan, Small, 2013, 9, 2905.
28 J. Feng, X. Sun, C. Wu, L. Peng, C. Lin, S. Hu, J. Yang and Y. Xie, J. Am. Chem. Soc., 2011, 133, 17832.
29 Xiao, J.; Zeng, X.; Chen, W.; Xiao, F.; Wang, S. Chem. Commun., 2013, 49, 11734–11736.
30 W. S. Hummers and R. E. Offeman, *J. Am. Chem. Soc.*, 1958, **80**, 1339.
31 D. Li, M. B. Muller, S. Gilje, R. B. Kaner and G. G. Wallace, *Nat. Nanotechnol.*, 2008, **3**, 101.
32 M. Shahid, N. Yesibolati, F. M. Ross, and H. N. Alshareef, *J. of Power Sources*, 2014, **263**, 239.
33 A. C. Ferrari and J. Robertson, *Phys. Rev. B*, 2000, **61**, 14095.
34 M. A. Pimenta, G. Dresselhaus, M. S. Dresselhaus, L. G. Canc ac... A. Jorioa and R. Saito, *Phys. Chem. Chem. Phys.*, 2007, **9**, 1276.
35 Z. –S. Wu, G. Zhou, L. –C. Yin, W. Ren, F. Li and H. –M. Cheng, *Nano Energy*, 2012, **1**, 107.
36 W. Du, Z. Wang, Z. Zhu, S. Hu, X. Zhu, Y. Shi, H. Pang and X. Qian, *J. Mater. Chem. A*, 2014, 2, 9613.
37 W. Du, Z. Wang, Z. Zhu, S. Hu, X. Zhu, Y. Shi, H.Pang, X. Qian, *J. Mater. Chem. A,* 2014, (in press).
38 J. Xiao, X. Zheng, W. Chen, F. Xiao and S. Wang, *Chem. commun.,* 2013, **49**, 11734.
39 J. Xiao, L. Wan, S. Yang, F. Xiao and S. Wang, *Nano Lett.,* 2014, **1**... 831.
40 M. Prabu, K. Keptpang, and S. Shanmugam *Nanoscale,* 2014, **6**, 3173.
41 Y. Ohno, *Phys. Rev. B*, 1991, **44**, 1281.